# Formation and geochemical significance of micrometallic aggregates including fissiogenic platinum group elements in the Oklo natural reactor, Gabon

Makiko Kikuchi[1], Hiroshi Hidaka[1]* and François Gauthier-Lafaye[2]

[1]Department of Earth and Planetary Systems Science, Hiroshima University, Higashi Hiroshima 739-8526, Japan

[2]Ecole et Observatoire des Sciences de la Terre, UMR7517-CNRS-UdS, 67084 Strasbourg, France

*Corresponding author

E-mail address: hidaka@hiroshima-u.ac.jp

Phone: (+81)82-424-7464

FAX: (+81)824-24-0735

**Abstract**

Metallic aggregates with a size of a few tens μm and consisting mainly of Ru, Rh, Pd, Te, Pb, As, Sb, S and Bi were found in the acid residue of SD37-S2/CD uraninite taken from Oklo natural reactor zone (RZ) 13. Quantitative analyses of major elements using an electron probe microanalyzer and *in situ* isotopic analyses of Zr, Mo, Ru, Pb and U using a sensitive high-resolution ion microprobe were performed on the metallic aggregates to determine the geochemical behaviors of fission products and actinides and to ascertain the processes of formation of the aggregates in the RZs. The chemical compositions of the aggregates investigated in this study are significantly different from those reported previously, showing lower Pb content and no correlation between the contents of Pb and S in the individual grains. The $^{235}U/^{238}U$ ratios in metallic aggregates vary significantly from 0.00478 to 0.01466, indicating chemical fractionation between U and Pu during the formation of the aggregates. The Pb isotopic data indicate that most of the Pb in the aggregates decayed from 2.05 Ga-old uraninite that existed in the RZ originally and that there was chemical fractionation between U and Pb in some aggregates. The Zr and Mo isotopic ratios, $^{90}Zr/^{91}Zr$ and $^{95}Mo/^{97}Mo$, for most of the aggregates had small variations, which can be simply explained by constant separate mixing of fissiogenic and nonfissiogenic components. On the other hand, a large variation in the $^{99}Ru/^{101}Ru$ ratio (0.324–1.73) cannot be explained only by a two-component mixing theory; thus, chemical fractionation between Tc and Ru during the reactor criticality is suggested. The large variations in the $^{235}U/^{238}U$ and $^{99}Ru/^{101}Ru$ isotopic ratios suggest that the aggregates formed under various redox conditions owing to the radiolysis of water.

## 1. INTRODUCTION

The long-term behavior of radioactive isotopes in the geosphere is of great interest in terms of establishing an underground nuclear waste repository. Studies of natural analogues in uranium and thorium deposits provide information on fixation and/or release processes of radioactive isotopes in geological formations over long periods of time (e.g., Cramer and Smellie, 1992; Maravic and Smellie, 1992). Among the natural analogues, the Oklo uranium deposit is considered a unique and important example because of the large-scale fission reactions that occurred 1.95 Ga ago (Gauthier-Lafaye et al., 1996).

Since the discovery of the first reactor zone (hereafter RZ) in 1972 (Bodu et al., 1972; Neuilly et al., 1972), 16 RZs have been identified in the Oklo uranium deposit and numbered in the chronological order of their discovery (Fig. 1(a)). Among these 16, RZs 1 to 9 were discovered during open pit mining operations and have since undergone considerable weathering under the prevailing oxidizing condition near the surface. On the other hand, RZs 10 to 16, which were discovered later, have experienced only a little weathering because they are located in an underground mine in a more reducing environment (Fig. 1(b)).

One of the major concerns is to identify the factors that control the mobility and retention of fission products in geological media. Radionuclide migration out of the RZs was caused mainly by three events. During the criticality, there was extensive hydrothermal alteration due to the heat of nuclear reactions (Gauthier-Lafaye et al., 1989). After the criticality, the RZs were altered 1000–700 Ma ago by regional extension and the intrusion of the Neoproterozoic dykes (Bonhomme et al., 1978; Gauthier-Lafaye et al., 1996; Evins et al., 2005), and finally by recent alteration and supergene weathering (Janeczek and Ewing, 1996a, 1996b; Stille et al., 2003).

The chemical states of fission products in artificially irradiated nuclear fuels obtained from elemental analyses have indicated that fissiogenic Mo, Tc, Ru, Rh, Pd, Ag, Cd, In, Sn, Sb and Te form metallic precipitates (Kleykamp, 1985). The first transmission electron microscope (TEM) observation of the alloy particles in light-water reactor spent fuel was performed by Thomas and Guenther (1989), and alloy particles referred to as epsilon phase were found to exist in the fuel-clad gap or at the boundaries of fuel grains. The chemical compositions of the epsilon phase extracted from spent fuel vary in a narrow range and the average composition (wt. %) is 32.7% Mo, 40.5% Ru, 7% Tc, 4.2% Rh, 11.7% Pd and 3.8% Te (Cui et al., 2004). Similar aggregates (in common parlance, metallic aggregates) have been found in RZs 10 and 13 of the Oklo uranium deposit (Gauthier-Lafaye et al., 1996; Hidaka et al., 1993, 1999; Utsunomiya and Ewing, 2006), and in sandstone below the Bangombé RZ (Janeczek, 1999). The aggregates consist of several fine minerals intergrown with galena (PbS) and U minerals (Gauthier-Lafaye et al., 1996). The sizes of the aggregates range from a few μm to 100 μm. In particular, larger-sized aggregates with diameters of ~100 μm were found in the sample SD37-S2/CD collected from RZ 13 (Gauthier-Lafaye et al., 1996). The chemical compositions of the aggregates found in RZ 13, determined by electron probe microanalysis (EPMA), are mainly Pb, Ru, Rh, Te, U, As and S, with the average composition (wt. %) being 38.89% Pb, 33.51% Ru, 4.64% Rh, 2.71% Te, 0.39% U, 7.99% As and 7.43% S (Hidaka et al., 1999). There is good correlation between the Ru-Rh-Te-As-S content and Pb-S content, suggesting that the aggregates are a mixture of these two components (Gauthier-Lafaye et al., 1996; Hidaka et al., 1999). Considering complexly mixed textures of the aggregates observed using a high-resolution TEM, Utsunomiya and Ewing (2006) suggested that dissolution and precipitation occurred within the aggregates in association with As-bearing and Pb-rich fluids.

Ru isotopic compositions of the Oklo samples can be used to deduce Tc behavior because $^{99}$Tc decays to $^{99}$Ru with a relatively long half-life of $2.1 \times 10^5$ years. $^{99}$Tc is an isotope of great concern in safety assessments of nuclear waste repositories as it can contribute significantly to the calculated dose for 10,000 years after repository closure (e.g., Chen et al., 2000). Previous isotopic studies of whole rocks using Oklo reactor samples indicated that the isotopic abundance of $^{99}$Ru expected from the experimentally obtained fission product yield deviates from the measurement values (Fréjacques et al., 1975; Curtis, 1986). The deviations of fissiogenic $^{99}$Ru can be interpreted as an addition or depletion of $^{99}$Tc, and suggest the occurrence of chemical fractionation between Ru and Tc in RZs. Although all of the $^{99}$Tc has already decayed to $^{99}$Ru at the Oklo site, the geological behavior of fissiogenic $^{99}$Tc in the RZs can be inferred from the isotopic composition of fissiogenic $^{99}$Ru. As the metallic aggregates in RZs constitute the host phase for large amounts of fissiogenic Mo, Ru, Rh and Pd, microscale analyses of the individual aggregates are necessary for further discussion. *In situ* isotopic analyses of the aggregates found in RZs 10 and 13 employing secondary ion mass spectrometry (Gauthier-Lafaye et al., 1996; Hidaka et al., 1993, 1999) revealed a more selective incorporation of $^{99}$Tc than Ru in the metallic aggregates.

There are scant data on Ru isotopic compositions of individual metallic aggregates. Therefore, the purpose of this study is to understand the long-term geological behavior of fission products and actinides such as Zr, Mo, Tc, Ru and U incorporated in the metallic aggregates from *in situ* isotopic analyses. Moreover, we propose to discuss the prevailing processes and conditions during the formation of metallic aggregates, as predicted from chemical and isotopic compositions measured in this study.

## 2. SAMPLE AND EXPERIMENTAL METHODS

## 2.1. Geological Setting

RZ 13 was discovered in 1984 at the south dome of the Oklo uranium deposit. Although RZ 13 is a small reactor that is 30 cm thick, 6 m wide and 10 m long, its vicinity has a very high uranium content (up to 87%) with highly depleted $^{235}U$ (down to $^{235}U/^{238}U$ = 0.0038) (Gauthier-Lafaye et al., 1996). RZ 13 exists between two galleries, SD35 and SD37. The sample SD37-S2/CD used in this study was collected from an area with the highest depletion of $^{235}U$ ($^{235}U/^{238}U$ = 0.004630) within the borehole SD37-S2 in RZ 13 (Holliger, 1993). The RZ is located 25 m south of the dolerite dyke dated 860 Ma (Evins et al., 2005). Large-scale U and Pb mobilization in RZ 13 influenced by the dolerite magma has been reported (Holliger, 1992, 1994; Nagy et al., 1993; Gauthier-Lafaye et al., 1996; Evins et al., 2005).

In an attempt to clarify the conflicting age estimates of the Oklo deposit, Gancarz (1978) measured the isotopic compositions of U and Pb in 10 U-rich ore samples that were located 2–8 m within the boundaries of the reactor zones. The data gave a formation age of the deposit of $(2.05 \pm 0.03) \times 10^9$ years. The age of the fission reaction was studied in detail using a bore-hole (SC36) that cuts across RZ 2 by comparing the fluence of the fission reaction to the amount of fission elements (mainly rare earth elements). The result was an age of 1950 ± 40 Ma (Ruffenach, 1978, 1979; Holliger, 1988; Naudet, 1991). The temperatures of the fluids in the reactors and during criticality have been the subject of many studies based on microthermometric measurements of fluid inclusions (Openshaw et al., 1978; Gauthier-Lafaye, 1986). Fluid inclusions in quartz overgrowths in sandstone adjacent to the RZ showed that the temperature reached 400°C and a convective hydrothermal system around the reactor started when fission reactions started (Gauthier-Lafaye et al., 1996). On the other hand, the $^{176}Lu/^{175}Lu$ ratio strongly depended on the average equilibrium temperature of neutrons at the time of reactor criticality

because the effective neutron capture cross-section of $^{176}$Lu is a sensitive indicator of temperature (Holliger and Devillers, 1981). The average temperature estimated from the $^{176}$Lu/$^{175}$Lu ratio was calculated to be 280°C ± 50°C. However, the calculated temperature is considered an underestimation owing to the migration of Lu during and after reactor operation and the uncertainty of the neutron capture cross-section of $^{175}$Lu (Gauthier-Lafaye et al., 1996; Hidaka and Holliger, 1998).

Significant differences between the nuclear characteristics of RZ 13 and those of other RZs are: (1) the proportion of $^{238}$U fission of SD37 is extremely high at 18% of the total fission, while proportions of other RZs are less than 5.0%; (2) the estimated criticality duration time of SD37-S2/CD is shorter ($2.42 \times 10^4$ years) than times of other RZs ($2.0–8.0 \times 10^5$ years), although the neutron fluence is nearly the same as fluences of other RZs (Hidaka and Holliger, 1998).

## 2.2. Sample Preparation

A few grams of SD37-S2/CD were leached with 2M $HNO_3$ to dissolve completely uraninite in the matrix, and the residues were collected for this study. These residues were then mounted on epoxy resin and polished with 1/4 μm diamond paste.

## 2.3. EPMA analysis

Before conducting a sensitive high-resolution ion microprobe (SHRIMP) analysis, EPMA (JEOL JXA-8200) was performed to quantitatively determine the major elements and obtain back-scattered electron (BSE) images of individual aggregates. The analytical spot size for the quantitative analysis was 2 μm, and the electron beam current was 20 nA at an acceleration voltage of 15 kV. The EPMA data were calibrated using reference materials consisting of pure metals (Ru, Rh, Pd, Te and Bi in ASTIMEX METM12-44)

and compounds ($UO_2$, GaAs, PbS, $CuFeS_2$, NiO and $Sb_2S_3$). The analysis lines and crystals used were Ru Lα, Rh Lα, Pd L β, Te Lα, Bi Mα, U M β, As Lα, Pb Mα, S Kα, Cu Kα, Ni Kα and Sb Lα and LiF for Ni and Cu, TAP for As and PET for Ru, Rh, Pd, Te, Bi, U, S, Pb and Sb. The average limits of detection were 240 ppm for Ru, 250 ppm for Rh, 430 ppm for Pd, 250 ppm for Te, 360 ppm for Bi, 410 ppm for U, 240 ppm for As, 370 ppm for Pb, 90 ppm for S, 350 ppm for Cu, 260 ppm for Ni and 250 ppm for Sb. As a result, 34 aggregates were identified by EPMA in this study. Figure 2 shows BSE images of typical metallic aggregates measured in this study. The BSE images indicate that the sizes of the aggregates range from <10 μm to 50 μm, and the aggregates seem to be polyphase grains consisting of fine particles smaller than the micron scale (Figs. 2(a) and (b)). Major elements of the aggregates are Ru, Rh, Pd, Te, Pb, As, S and Bi. In addition, the existence of U, Sb, Ni and Cu as minor elements in the aggregates was confirmed.

**2.4. SHRIMP analysis**

Although the concentrations of Mo and Zr in the aggregates were below the detection limit of quantitative EPMA (less than 0.01 wt.%), they could be measured through SHRIMP analysis. In this study, 14 relatively large aggregates (larger than 20 μm) were selected from 34 aggregates for *in situ* isotopic analysis. The isotopic analyses of Zr, Mo, Ru, Pb and U were performed using SHRIMP II at Hiroshima University. A nA scale beam of $O_2^-$ primary ions was used to sputter a 5 μm analytical spot on the individual aggregates. The peaks of $^{90}$Zr, $^{91}$Zr, $^{92}$Zr+$^{92}$Mo, $^{94}$Zr+$^{94}$Mo, $^{95}$Mo, $^{96}$Zr+$^{96}$Mo+$^{96}$Ru, $^{97}$Mo, $^{98}$Mo+$^{98}$Ru, $^{99}$Ru, $^{100}$Mo+$^{100}$Ru, $^{101}$Ru, $^{102}$Ru+$^{102}$Pd, $^{104}$Ru+$^{104}$Pd, $^{204}$Pb, $^{206}$Pb, $^{207}$Pb, $^{208}$Pb, $^{235}$U and $^{238}$U were measured with a mass resolution of 5800 (M/ΔM at 1% of the peak height) using a 80 μm wide source slit and a 100 μm wide

collector slit.

An ASTIMEX metal standard mount METM 25-42 was used as the standard material of nonfissiogenic isotopes, and isotopic analyses in terms of Zr, Mo and Ru were performed to confirm the analytical precision and the instrumental mass fractionation. Since the mass numbers of 92, 94, 96, 98, 100, 102 and 104 have isobaric interference for Zr, Mo and Ru isotopic measurements in SHRIMP analysis, only the isotopic ratios of $^{90}Zr/^{91}Zr$, $^{97}Mo/^{95}Mo$ and $^{99}Ru/^{101}Ru$ are discussed in this study. The isotopic ratios, $^{91}Zr/^{90}Zr$, $^{97}Mo/^{95}Mo$ and $^{99}Ru/^{101}Ru$, in the standard materials were corrected for instrumental mass fractionation by an exponential law using the values of $^{94}Zr/^{90}Zr$ = 0.3381, $^{96}Mo/^{95}Mo$ = 1.0527 and $^{96}Ru/^{101}Ru$ = 0.3249 as normalization factors (Minster and Ricard, 1981; Poths et al., 1987; Wieser et al., 2007). For the convenience of comparing with previous isotopic data (Hidaka et al., 1994; Bros et al., 2003), the Zr isotopic data were finally treated as $^{90}Zr/^{91}Zr$ after conversion from $^{91}Zr/^{90}Zr$.

Only after the analyses for Zr, Mo and Ru were conducted, Pb and U isotopic analyses were performed separately. For Pb and U isotopic analyses, NIST SRM610 glass was used as the standard material. In the case of U isotopic analysis, AS3 standard zircon ($^{235}U/^{238}U$ = 0.00725 ± 0.00004) was also measured to check the terrestrial U isotopic ratio.

## 3. RESULTS

### 3.1. Chemical Compositions of Metallic Aggregates

Twenty-two analytical spots from 14 typical metallic aggregates were selected for EPMA analyses in this study. The data of the chemical compositions are presented in Table 1. Typical two data previously obtained for metallic aggregates in RZs 10 and 13 (Gauthier-Lafaye et al., 1996; Hidaka et al., 1999) are also presented for comparison. The

chemical compositions of the aggregates investigated in this study are significantly different from those for RZs 10 and 13 reported previously. In this study, we used the same sample SD37-S2/CD that was used previously to find metallic aggregates (Hidaka et al., 1999). This suggests that the heterogeneity of the metallic aggregates in the sample is extremely high.

The Pb contents in the aggregates (1.24–4.49 wt.%) found in this study are lower than those of other aggregates in RZs 10 and 13 (14.16–59.02 wt.%) reported previously. Hidaka et al. (1999) reported the data of chemical compositions of individual aggregates in RZ 13, and demonstrated a good correlation between Ru+Rh+Te+As+S and PbS components. Therefore, the metallic aggregates are considered to have been formed by the mixing of two end-members: one component being mainly Ru, Rh and Te produced by fission and the other being galena existing in the RZ uraninite. However, the aggregates found in this study show no correlation between the contents of Pb and S, which suggests that the Pb does not exist in the aggregates as galena. A positive correlation between the contents of Pb and U was observed in this study. This result implies that a major part of the Pb in the aggregates found in this study might be radiogenic Pb derived from U.

The fundamental difference between metallic aggregates in natural reactors and epsilon phase in spent fuel is their chemical forms; the metallic aggregates are bound to As or S (or both), while the epsilon phase has a metallic bond (e.g., Janeczek, 1999). The metallic aggregates have been considered to be affected by hydrothermal fluids bearing As, S and other trace metals derived from the criticality and/or intrusion of dolerite dyke (Utsunomiya and Ewing, 2006). In previously reported studies, all of the metallic aggregates found in RZs 10 and 13 have shown a positive correlation among Ru-, Rh- and Pd-As (Gauthier-Lafaye et al., 1996; Hidaka et al., 1999). However, the aggregates

investigated in this study show different trends among the concentrations of Ru, Rh, Pd and As. The concentration of Ru has a clear negative correlation with that of As (Fig. 3(a)), while that of Pd has a positive correlation with that of As (Fig. 3(b)). The concentration of Rh has no correlation with that of As. These results suggest that the fissiogenic Ru, Rh and Pd have different chemical behaviors in the aggregates. The concentration of Ru in the aggregates has a clear positive correlation with that of Cu (Fig. 3(c)). The concentrations of Ru and Cu have negative correlations with the concentration of As and no discernible correlation with the concentration of S. Therefore, we can reasonably surmise that Ru and Cu might exist in the aggregates as an alloy. Judging from the correlations of elements, two main phases might compose the metallic aggregates found in this study: Ru-Cu phase and Rh-Pd-Te-Pb-U-As-S-Bi-Sb-Ni phase (Fig. 3(d)). In the Rh-Pd-Te-Pb-U-As-S-Bi-Sb-Ni phase, Rh has coexisted with Te and S (Figs. 3(e) and (f)), and Pd has coexisted with As, Bi, Pb, U and Sb. On the other hand, the concentration of As is also positively correlated with the concentrations of Te and Ni (Figs. 3(g) and (h)). Therefore, it is possible that some phases have congregated in the As-bearing phase in the aggregates in a complicated manner.

The average ratios of Ru/Rh/Te in RZs 10 and 13 have been reported as 36/7/1 and 12/2/1 (Te = 1), respectively (Gauthier-Lafaye et al., 1996; Hidaka et al., 1999), which would reflect the conditions of the reactor operation and the degrees of alteration by thermal events through intrusion of the dolerite dyke. The average ratio of Ru/Rh/Te in the aggregates observed in this study is 13/2/1. Although the chemical compositions differ between the aggregates in this work and those in the work of Hidaka et al. (1999), especially the contents of Pb and S, the ratios of Ru/Rh/Te are almost the same. This suggests that the effects of hydrothermal fluid that led to the migration of Pb and the precipitation of PbS would have been different in the local area of RZ 13 while the

fissiogenic Ru, Rh and Te have been well preserved in the aggregates since they were formed.

### 3.2. Isotope Distribution in Metallic Aggregates Determined by *In Situ* SHRIMP Analysis

#### *3.2.1. Uranium*

The $^{235}U/^{238}U$ isotopic ratios in 14 metallic aggregates of RZ 13 measured in this study are presented in Table 2 and plotted in Fig. 4. The $^{235}U/^{238}U$ ratios of metallic aggregates (0.00478–0.01466) have large variations compared with the standard value (0.00725). Depletion of $^{235}U$ is commonly observed in and around the RZs because of the consumption of $^{235}U$ by fission. Besides the depleted $^{235}U/^{238}U$ in the whole rock sample SD37-S2/CD, two metallic aggregates found in RZ 13 also show depleted $^{235}U/^{238}U$ of the order of 0.0038 (Gauthier-Lafaye et al., 1996). The enriched $^{235}U/^{238}U$ ratios have been observed only in a few samples of clay minerals and apatite, around the reactor zone (Bros et al., 1993, 1996; Horie et al., 2004). In the Oklo RZs, $^{239}Pu$ was produced by fast neutron capture of $^{238}U$. The presence of excess $^{235}U$ has been explained by the mechanism of selective incorporation of $^{239}Pu$ into specific minerals after the incidence of chemical fractionation between U and Pu, as $^{239}Pu$ decays to $^{235}U$ with a half-life of $2.4 \times 10^4$ years (Bros et al., 1993, 1996; Horie et al., 2004). The enriched $^{235}U/^{238}U$ isotopic ratio observed in apatite around RZ 10 has been explained by the chemical fractionation between U and Pu in an oxidizing condition made possible by a rise in the concentration of radiolytic oxygen (Horie et al., 2004).

#### *3.2.2. Lead*

As described in section 3.1, the metallic aggregates investigated in this study have

extremely low Pb contents and a portion of Pb in the aggregates might be of radiogenic origin from RZ uraninite. This result may provide a clue to understanding the formation processes of the metallic aggregates, as the aggregates investigated in this study appear to have been formed under a different condition or at a different time compared with the previously found aggregates. The chronological interpretation of Pb-Pb data in the Oklo samples is complicated owing to the significant mobilization of Pb due to the intrusion of the dolerite dyke (Gauthier-Lafaye et al., 1996). Therefore, only a detailed comparison of the Pb isotopic data would make a discussion on the origin of the Pb component in the metallic aggregates possible.

The Pb isotopic data of 12 metallic aggregates are presented in Table 2 along with the previously generated data of aggregates in SD37-S2/CD (Gauthier-Lafaye et al., 1996). Moreover, to ascertain the evolutionary history of Pb isotopes, the $^{204}Pb/^{206}Pb$ vs. $^{207}Pb/^{206}Pb$ data of the metallic aggregates are plotted in Fig. 5. The Pb in metallic aggregates at the Oklo site is assumed to have had two modes of origins: (1) Pb originated from galena, which originally existed in uraninite matrices and/or was precipitated by the thermal event accompanied by the intrusion of the dolerite dyke, and (2) radiogenic Pb was derived from RZ uraninite. The Pb isotopic data of galena and uraninite in RZ 13 are also plotted in Fig. 5 for comparison. As shown in Table 2 and Fig. 5, all of the $^{207}Pb/^{206}Pb$ and $^{208}Pb/^{206}Pb$ isotopic ratios in this study (0.091–0.121 and 0.00715–0.00894, respectively) are lower than those of the aggregates reported previously (0.1259–0.1266 and 0.01376–0.01413, respectively) and galena (0.12990 and 0.01382, respectively) in SD37-S2/CD. The difference in Pb isotopic ratios was perhaps due to the mode of origin of Pb in the aggregates. The lower $^{204}Pb/^{206}Pb$, $^{207}Pb/^{206}Pb$ and $^{208}Pb/^{206}Pb$ isotopic ratios observed in the aggregates found in this study are similar to those of the native lead found in RZs (0.00012–0.00013, 0.10160–0.10170 and

0.00613–0.00614, respectively), which are also plotted in Fig. 5 for comparison. Native lead has been found in RZs 10 and 13 and is considered to contain radiogenic lead from highly depleted $^{235}U$ (Gauthier-Lafaye et al., 1996). Since the Pb in the aggregates does not bond to S and may be radiogenic Pb derived from U, the mode of origin of Pb in some aggregates having depleted $^{235}U$ is considered similar to that of native lead.

*3.2.3. Zirconium*

Zr has five stable isotopes with mass numbers of 90, 91, 92, 94 and 96, and all are produced by fission. The $^{90}Zr/^{91}Zr$ ratios obtained in 14 metallic aggregates are presented in Table 3 and Fig. 7(a), together with isotopic ratios of fissiogenic and nonfissiogenic Zr. Fissiogenic $^{90}Zr/^{91}Zr$ = 0.9456 presented in Table 3 is calculated from the fission yield of $^{90}Zr$ relative to $^{91}Zr$ (England and Rider, 1988) after taking into consideration the fission inventory for $^{235}U$, $^{238}U$ and $^{239}Pu$ in SD37-S2/CD (Hidaka et al., 1999). The $^{90}Zr/^{91}Zr$ ratios of metallic aggregates (1.648–2.651) show that the $^{90}Zr/^{91}Zr$ data of the aggregates are between fissiogenic and nonfissiogenic $^{90}Zr/^{91}Zr$ ratios (0.9456 and 4.659, respectively). This result indicates that the Zr isotopic compositions in the aggregates are attributed to a mixture of two components: nonfissiogenic Zr from native material and fissiogenic Zr from RZ material. However, the data of three analytical spots (metallic aggregates 2-1, 2-2 and 3-2) show significant excess of the $^{90}Zr$ isotope. The BSE image of metallic aggregates 2-1 and 2-2 in Fig. 2(a) shows the existence of microinclusions in the aggregates. Moreover, the existence of silicates of U and Zr has been reported in the aggregates found in RZ 10 (Gauthier-Lafaye et al., 1996). Therefore, the mixing ratios of fissiogenic and native Zr might be different in such an inclusion from those of Ru-, Rh- and Pd-rich regions.

*3.2.4. Molybdenum*

The $^{97}Mo/^{95}Mo$ isotopic ratios for 14 metallic aggregates are presented in Table 3 and Fig. 7(b). The results indicate that the Mo isotopic compositions ($^{97}Mo/^{95}Mo$ = 0.817 ± 0.005–0.932 ± 0.005) are due to mixing between fissiogenic and nonfissiogenic Mo ($^{97}Mo/^{95}Mo$ = 0.9768 and 0.5986 ± 0.0002). In addition, the $^{97}Mo/^{95}Mo$ isotopic ratios are consistent among all aggregates. This consistency suggests that the mixing ratios of fissiogenic and nonfissiogenic Mo were the same in all metallic aggregates.

*3.2.5. Ruthenium*

Ru is a minor element in common crustal rock, but is present in high quantities in RZs because of the high fission yields of Ru (Loss et al., 1989). Ru has seven stable isotopes with mass numbers of 96, 98, 99, 100, 101, 102 and 104. Among these seven Ru isotopes, $^{99}Ru$, $^{101}Ru$, $^{102}Ru$ and $^{104}Ru$ are produced by fission, while $^{96}Ru$, $^{98}Ru$ and $^{100}Ru$ (shielded by $^{96}Zr$, $^{98}Zr$ and $^{100}Mo$, respectively) are not produced in any appreciable quantity by fission. The $^{99}Ru/^{101}Ru$ isotopic ratios measured in this study are presented in Table 3 and Fig. 7(c). Figure 7(c) also contains a plot of the expected fissiogenic and nonfissiogenic $^{99}Ru/^{101}Ru$ (0.7550 and 1.136). The figure shows significant deviations of the $^{99}Ru/^{101}Ru$ ratios measured in this study from the expected values assumed from mixing between the expected fissiogenic and nonfissiogenic $^{99}Ru/^{101}Ru$. The deviations of $^{99}Ru/^{101}Ru$ ratios from the expected fissiogenic value in the Oklo samples have been recognized to be a result of chemical fractionation between Ru and Tc, as $^{99}Ru$ is produced by $^{99}Tc$ with a relatively long half-life of $2.1 \times 10^5$ years (e.g., Fréjacques et al., 1975; Curtis, 1986; Hidaka et al., 1993, 1999). Indeed, the metallic aggregates reported by Hidaka et al. (1993) have shown the presence of enriched $^{99}Ru/^{101}Ru$, the existence of which is interpreted as a case of selective uptake of $^{99}Tc$ into metallic aggregates under a

reducing condition. On the other hand, the depleted $^{99}Ru/^{101}Ru$ in the metallic aggregates has never been reported. An isotopic enrichment and depletion of $^{99}Ru$ have been observed in uraninite matrices (Hidaka et al., 1993, 1999). Such a variation of the $^{99}Ru$ isotopic abundance in uraninite samples is considered to have been caused by the presence of a local oxidizing condition in $UO_2$ matrix due to the radiolysis of water (Savary and Pagel, 1997). The U isotopic ratios in the aggregates investigated in this study suggest that the aggregates might have been affected by the radiolysis of water and that the redox conditions changed locally. The variation in $^{99}Ru/^{101}Ru$ confirms a change in the redox condition in the aggregates during the reactor operation.

## 4. DISCUSSION

### 4.1. Effect of the Radiolysis of Water

Radiolysis of water is commonly observed when the spent fuel is directly exposed to groundwater, where both oxidants (OH*, $H_2O_2$, $HO_2$* and $O_2$) and reductants (hydrated electrons ($e_{aq}^-$), H* and $H_2$) are produced. Interestingly, the radiolysis of water being effectively catalyzed by Pd (as a model for noble metal particles) has been reported (Nilsson and Jonsson, 2008). Therefore, radiolysis of water in the metallic aggregates in the natural reactors is envisaged, and this reaction has led to oxidizing and reducing conditions inside the aggregates.

### 4.2. Chemical Fractionation

#### *4.2.1. U and Pu*

Aggregates that contain O, Zr, Mo, Ru, Pd, U and Pu have been observed in spent fuel (Buck et al., 2004). The individual particles forming the aggregates are only a few μm across, and the particles that contain O, Zr, U and Pu are mixed within the aggregates.

Likewise, the metallic aggregates could well have incorporated a part of the RZ uraninite containing O, Zr, U and Pu during their formation. U rather than Pu very likely underwent selective dissolution within the oxidized area owing to the radiolysis of water in the aggregates, which resulted in chemical fractionation between U and Pu. The ratios of chemical fractionation between U and Pu could have led to the heterogeneous distribution of $^{235}U$ and depletion and enrichment of $^{235}U/^{238}U$ in the aggregates.

*4.2.2. U and Pb*

U in the aggregates is considered to have been derived from the 2.05 Ga-old uraninite in RZ. The incorporation of the 2.05 Ga-old uraninite of RZ in the metallic aggregates perhaps occurred 1.95 Ga ago when the fission chain reactions of $^{235}U$ were initiated and the formation of fissiogenic platinum group element (PGE) particles began. The chemical fractionation between U and Pu must have completed during the reactor operation because of the short half-life of $^{239}Pu$. After the chemical fractionation, the radiogenic Pb isotopic compositions should vary depending on the $^{235}U/^{238}U$ isotopic ratio. $^{235}U/^{238}U$ vs. $^{207}Pb/^{206}Pb$ of the metallic aggregates is plotted in Fig. 6. In the absence of chemical fractionation between U and Pb since the deposition of the Oklo uraninite 2.05 Ga ago, the $^{207}Pb/^{206}Pb$ isotopic ratio of the aggregates can be expressed as a function of the $^{235}U/^{238}U$ isotopic ratio:

$$\left(\frac{^{207}Pb}{^{206}Pb}\right) = \left(\frac{^{207}Pb}{^{206}Pb}\right)_{2.05\ Ga} - \left(\frac{^{235}U}{^{238}U}\right)_n \cdot \frac{\exp(\lambda_5 t) - 1}{\exp(\lambda_8 t) - 1} + \left(\frac{^{235}U}{^{238}U}\right) \cdot \frac{\exp(\lambda_5 t) - 1}{\exp(\lambda_8 t) - 1},$$

where ($^{207}Pb/^{206}Pb$) is the calculated $^{207}Pb/^{206}Pb$ ratio of the metallic aggregates, $(^{207}Pb/^{206}Pb)_{2.05\ Ga}$ = $^{207}Pb/^{206}Pb$ is derived from normal U for 2.05 billion years after the consideration of common lead ($^{206}Pb/^{204}Pb$ = 18.61, $^{207}Pb/^{204}Pb$ = 15.74 (Mathieu et al., 2001)), $(^{235}U/^{238}U)_n$ is the normal $^{235}U/^{238}U$ ratio, $\lambda_5$ is the decay constant of $^{235}U$, $\lambda_8$ is the

decay constant of $^{238}U$, t is the age of the criticality ($1.95 \times 10^9$ a), and $^{235}U/^{238}U$ is the varying $^{235}U/^{238}U$ ratio.

The calculated $^{207}Pb/^{206}Pb$ values are shown in Fig. 6 and are seen to increase linearly with $^{235}U/^{238}U$ (see the line denoted "f = 1" in Fig. 6). Although the $^{207}Pb/^{206}Pb$ ratios of the aggregates measured in this study have a positive correlation with $^{235}U/^{238}U$ ratios, the measured values deviate from the calculated values as the $^{235}U/^{238}U$ ratio rises. The deviations of the measured values from the calculated values can be explained by various degrees of chemical fractionation between U and Pb in each aggregate. The possible major events that led to U–Pb chemical fractionation are considered to have occurred during the reactor operation 1.95 Ga ago and/or during the intrusion of the dolerite dyke 0.86 Ga ago (Utsunomiya and Ewing, 2006). However, our result in Fig. 6 suggests the occurrence of U–Pb fractionation during the reactor operation because the deviations between measured and calculated values increase with an increase in the $^{235}U/^{238}U$ ratio. As described in section 3.2.1, the $^{235}U/^{238}U$ ratios of the aggregates changed with the degree of chemical fractionation between U and Pu under various redox conditions during the reactor operation. Since the chemical behaviors of U and Pb differ, the occurrence of chemical fractionation between U and Pb during the dissolution of U from the aggregates is considered reasonable. Assuming that the chemical fractionation between U and Pb occurred during the reactor operation, the $^{207}Pb/^{206}Pb$ isotopic ratio of the aggregates can be calculated as

$$\left(\frac{^{207}Pb}{^{206}Pb}\right)_f = \left(\frac{^{207}Pb}{^{206}Pb}\right) \times f + \left(\frac{^{207}Pb}{^{206}Pb}\right)_{Pb} \times (1-f)$$

$$\left(\frac{^{207}Pb}{^{206}Pb}\right)_{Pb} = \left(\frac{^{207}Pb}{^{206}Pb}\right)_{2.05\ Ga} - \left(\frac{^{235}U}{^{238}U}\right)_n \cdot \frac{\exp(\lambda_5 t) - 1}{\exp(\lambda_8 t) - 1},$$

where $(^{207}Pb/^{206}Pb)_f$ is the calculated $^{207}Pb/^{206}Pb$ ratio of the metallic aggregates during chemical fractionation between U and Pb 1.95 Ga ago, f is the proportion of the

nonfractionated U and Pb component relative to the total fraction, ($^{207}Pb/^{206}Pb$) is the nonfractionated U and Pb component, and $(^{207}Pb/^{206}Pb)_{Pb}$ is the fractionated Pb component 1.95 Ga ago. The $(^{207}Pb/^{206}Pb)_f$ values calculated using f = 0.3, 0.5, 0.8 and 1 (nonfractionated value) are shown in Fig. 6. In the figure, the aggregates having $^{235}U/^{238}U$ = 0.004 to 0.005 indicate that there was no chemical fractionation between U and Pb, and their $^{207}Pb/^{206}Pb$ apparent ages are from 2.01 ± 0.24 to 2.30 ± 0.18 Ga (metallic aggregates 1-1, 1-2, 10-1, 13-1 and 13-2 in Table 2), which roughly correspond to the depositional age of the uraninite at Oklo dated 2.05 Ga. The $^{207}Pb/^{206}Pb$ ratio of one analytical spot with $^{235}U/^{238}U$ = 0.00497 (metallic aggregate 5-1 in Table 2) is higher than the calculated value, and its $^{207}Pb/^{206}Pb$ apparent age is 2.41 ± 0.08 Ga. As shown in Table 2, metallic aggregate 5 (5-1 and 5-2) exhibits depletion as well as enrichment of $^{235}U/^{238}U$, which demonstrates heterogeneous distributions of $^{235}U/^{238}U$ and radiogenic $^{207}Pb/^{206}Pb$ on a microscale. Therefore, it is difficult to demonstrate an accurate relationship between Pb and U isotopic compositions using the data from metallic aggregate 5 (5-1 and 5-2). On the other hand, chemical fractionation between U and Pb in the aggregates having $^{235}U/^{238}U$ > 0.007 was observed. In Fig. 6, the data point having the highest $^{235}U/^{238}U$ (0.01466) is plotted in the area of f = 0.3–0.4. This result demonstrates that the $^{207}Pb/^{206}Pb$ present in the aggregate that underwent the most severe chemical fractionation was derived from the mixing of two components, one being the nonfractionated U-Pb (30%–40%) and the other being the fractionated U-Pb (60%–70%).

### 4.3. Effects of Leaching on Metallic Aggregates

The differences in redox conditions strongly affect the dissolution rates of Mo, Tc, Ru, Rh and Pd in metallic aggregates (e.g., Forsyth, 1996; Cui et al., 2001, 2004). Leaching experiments on Mo-Ru-Tc-Pd-Rh-Te alloy particles extracted from spent fuel

have demonstrated similar rates of leaching for $^{99}$Tc and $^{100}$Mo (1.5 ppb/day), which are three orders of magnitudes higher than those for Ru, Rh and Pd. Moreover, the rate of leaching of the epsilon phase under an oxidizing condition is ~100 times that under a reducing condition.

*4.3.1. Mo*

The chemical compositions of the epsilon phase in spent nuclear fuel indicate that fissiogenic Mo has the highest abundance of 40 wt% among fissiogenic Mo, Tc, Ru, Rh and Pd (e.g., Cui et al., 2004). However, inclusion of Mo in the metallic aggregates found in RZs has never been reported (Gauthier-Lafaye et al., 1996; Hidaka et al., 1999). Since Mo has a high fission yield, large amounts of fissiogenic Mo are expected to have been produced in the RZs and incorporated into the metallic aggregates during the reactor criticality. In this study, however, EPMA analysis revealed a low Mo concentration under the limit of detection (hundreds of ppm) in the aggregates. The low concentration of Mo in the aggregates found at the Oklo site is probably due to the partial leaching of Mo from the metallic aggregates under reducing conditions (Cui et al., 2001, 2004). According to Hidaka et al. (1999), the metallic aggregates in SD37-S2/CD formed during reactor operation. Therefore, the length of time over which Mo leached from the aggregates might be about two billion years. A calculation of the leached amounts of Mo during the aforesaid period of two billion years using a leaching rate of 1.5 ppb/day shows the total leached amounts exceed the total Mo content in the epsilon phase (about 40 wt.%). This result implies that Mo in the aggregates should have leached out entirely during the previously mentioned two billion years even under a reducing condition. However, the presence of some Mo has been identified in SHRIMP analyses in this study. The difference between expected and measured values of the concentrations of Mo suggests

the leaching of fissiogenic Mo out of the aggregates.

*4.3.2. Tc*

Under changing redox conditions, two factors probably affect the chemical fractionation between Tc and Ru: (1) the incorporating ratios of Tc and Ru during formation of metallic aggregates, and (2) the rates of leaching of Tc and Ru during and after formation. Taking into account the half-life of $2.1 \times 10^5$ years for $^{99}$Tc, the fractionation between Tc and Ru must have occurred over a period of ~$2.1 \times 10^5$ years. In such a relatively long period of time, the $^{99}$Ru/$^{101}$Ru ratios should be strongly affected by the leaching behavior of $^{99}$Tc. As shown in section 3.2.4, the rate of leaching of Tc is $10^3$–$10^4$ times that of Ru even under a reducing condition, and is about 1.5 ppb/day. Considering the length of time of ~$2.1 \times 10^5$ years over which $^{99}$Tc leached, the total amount of leached $^{99}$Tc is estimated as ~$1.2 \times 10^5$ ppm under a reducing condition. The lowest $^{99}$Ru/$^{101}$Ru ratio observed in this study is $0.324 \pm 0.001$, which indicates that the total amount of leached $^{99}$Tc was the highest in all metallic aggregates. Assuming that the rate of leaching of $^{99}$Tc under an oxidizing condition is ~100 times that under a reducing condition, the $^{99}$Ru/$^{101}$Ru ratios of the aggregates decrease to 0.324.

**4.4. Formation Processes of Metallic Aggregates**

Summarizing the results and discussions in this study, the formation processes of the metallic aggregates at SD37-S2/CD in RZ13 can be described as follows (Fig. 8). (i) The fissiogenic Mo, Tc, Ru, Rh, Pd and Te formed fine particles (less than a few μm in size) during the criticality and were gathered at the grain boundaries of 2.05 Ga-old $UO_2$ matrix. At the same time, the hydrothermal fluid including As, S, Te, Bi, Sb, Ni and Cu started to circulate in and around the RZ, which altered and dissolved the original

fissiogenic PGE particles and $UO_2$ matrix. Through interaction between the fissiogenic PGE particles and hydrothermal fluid, the metallic aggregates (a few tens of microns to 100 μm in size) formed having two main end-members where the fissiogenic Ru bonded to Cu while Rh and Pd formed complicated phases with As, S, Te, Bi, Sb and Ni. In addition, the 2.05-Ga fine uraninite grains including U, Pu, Zr and radiogenic Pb might have been derived from the alteration of $UO_2$ matrix and incorporated in the aggregates. (ii) During the criticality, there were oxidizing and reducing conditions due to the radiolysis of water inside the metallic aggregates. In the oxidizing regions, U, Mo and Tc might have leached from the aggregates, which led to the chemical fractionations between U and Pu, U and Pb, and Tc and Ru in the aggregates. (iii) Subsequently, the second hydrothermal fluid was derived from intrusion of the dolerite dyke 0.86 Ga ago at the Oklo site. Since this thermal event is considered to have mobilized a large amount of Pb and U, the radiogenic Pb accumulated in the $UO_2$ matrix could dissolve in the fluid and produce the Pb-rich hydrothermal fluid. Such Pb-rich fluid has been considered to lead to the precipitations of galena in the $UO_2$ matrix and metallic aggregates and to form the PbS-rich metallic aggregates observed in previous works. However, the absence of PbS in the aggregates studied in this work suggests that the aggregates were not affected by the Pb-rich fluids. Therefore, the degrees of interaction between the hydrothermal fluid and metallic aggregates could be different in the local area of SD37-S2/CD in RZ 13 during intrusion of the dolerite dyke.

## 5. CONCLUSIONS

The chemical compositions of the metallic aggregates investigated in this study are quite different from those for aggregates reported previously. In the absence of any discernible correlation between Pb and S and in the existence of a positive correlation

between U and Pb in the aggregates, the source of Pb in the aggregates is considered to be RZ uraninite and not galena. Although the $^{235}U/^{238}U$ isotopic ratios observed in the RZ are generally depleted, the $^{235}U/^{238}U$ isotopic ratios of the aggregates show enrichment as well as depletion. The variable $^{235}U/^{238}U$ ratio suggests that the aggregates were affected by the radiolysis of water, and there was large chemical fractionation between U and Pu in RZ 13 during criticality. The Pb isotopic ratios demonstrate that most of the Pb components in metallic aggregates were formed by radiogenic Pb derived from RZ uraninite. The deviation of the $^{207}Pb/^{206}Pb$ isotopic ratio from the expected value suggests the occurrence of radiogenic Pb and U in an incomplete chemical fractionation during the criticality. The isotopic data of the aggregates indicate that Zr and Mo isotopic compositions of metallic aggregates can be explained by the mixing of fissiogenic and nonfissiogenic components. However, the $^{99}Ru/^{101}Ru$ isotopic ratios of the aggregates show enrichment as well as depletion in each aggregate, which cannot be explained by the mixing of fissiogenic and nonfissiogenic components. The variations of $^{99}Ru/^{101}Ru$ ratios are considered to be a result of the incorporation of Tc and Ru in various ratios after chemical fractionation between Tc and Ru during reactor operation. The large variations in the $^{99}Ru/^{101}Ru$ and $^{235}U/^{238}U$ ratios probably suggest that the aggregates formed under various redox conditions owing to the radiolysis of water.

## Acknowledgments

We are very grateful for the critical reading of the manuscript by Drs. P. Stille, R. D. Loss and an anonymous reviewer. This study was financially supported by a Research Fellowship for Young Scientists (to M.K., No. 19_8344) and a Grant-in-Aid for Scientific Research (to H.H., No. 21244086) from the Japan Society for the Promotion of Science.

## REFERENCES

Bodu R., Bouzigues H., Morin N. and Pfiffelmann J. P. (1972) Sur l'existence d'anomalies isotopiques rencontrées dans l'uranium du Gabon. *C. R. Acad. Sci. Paris* **275,** 1731–1734.

Bonhomme M., Gauthier-Lafaye F., and Weber F. (1982) An example of Lower Proterozoic sediments: The Francevillian in Gabon. *J. Precam. Res.* **18,** 87–102.

Bros R., Gauthier-Lafaye F., Holliger P. and Still P. (1993) Occurrence of naturally enriched $^{235}$U: Implications for plutonium behavior in natural environments. *Geochim. Cosmochim. Acta* **57**, 1351–1356.

Bros R., Carpena J., Sere V. and Beltritti A. (1996) Occurrence of Pu and fissiogenic rare earth elements in hydrothermal apatites from the fossil natural nuclear reactor 16 of Oklo (Gabon). *Radiochim. Acta* **74**, 277–282.

Bros R.**,** Hidaka H., Kamei G. and Ohnuki T. (2003) Mobilization and mechanisms of retardation in the Oklo natural reactor zone 2 (Gabon)—inferences from U, REE, Zr, Mo and Se isotopes. *App. Geochem.* **18**, 1807–1824.

Buck E. C., Hanson B. D. and McNamara B. K. (2004) The geochemical behavior of Tc, Np and Pu in spent nuclear fuel in an oxidizing environment. In *Energy, Waste, and the Environment: a Geochemical Perspective* (eds. R. Gieré, P. Stille). The Geological Society of London Special Publication 236, pp. 65–88.

Chen F., Burns P. C. and Ewing R. C. (2000) Near-field behavior of $^{99}$Tc during the oxidative alteration of spent nuclear fuel. *J. Nucl. Mat.***278**, 225–232.

Cramer J. J. and Smellie J. A. T. (1992) The AECL/SKB Cigar Lake analogue study. Some implications for performance assessment, EUR proceedings of the 5th CEC Natural Analogue Working Group, Toledo, Spain. Oct. 6–9.

Cui D., Eriksen T. and Eklund U. B. (2001) On metal aggregates in spent fuel, synthesis and leaching of Mo-Ru-Pd-Rh Alloy. *In Scientific Basis for Nuclear Waste Management XXIV.* (eds. K. P. Hart and G. R. Lumpkin) *Mater. Res. Soc. Symp. Proc.* **663**, 427.

Cui D., Low J., Sjöstedt C. J. and Spahiu, K. (2004) On Mo-Ru-Tc-Pd-Rh-Te alloy particles extracted from spent fuel and their leaching behavior under Ar and $H_2$ atmosphere. *Radiochim. Acta* **92**, 551-555.

Curtis D. (1986) Geochemical controls on 99-Tc transport and retention. *Chem. Geol.* **55**, 227–231.

England T. R. and Rider B. F. (1988) Chainy for MITO-TAL, Los Alamos National Laboratory Report, LA-UR-88-1696.

Evins L. Z., Jensen K. A. and Ewing R. C. (2005) Uraninite recrystallization and Pb loss in the Oklo and Bangombé natural fission reactors, Gabon. *Geochim. Cosmochim. Acta* **69**, 1589–1606.

Forsyth R. S. (1996) Spent fuel corrosion: Study of the Tc-99 source term for the BWR and PWR reference fuel. SKB arbete report 94–07.

Fréjacques C., Blain C., Devillers C., Hagemann R. and Ruffenach J. C. (1975) Conclusions tirés de l'etude de la migration des produits de fission. *Le phénomène d'Oklo*, pp. 509–524, IAEA.

Gancarz A. J. (1978) U-Pb age ($2.05 \times 10^9$ years) of the Oklo uranium deposit. *In Natural Fission Reactors*, pp. 513–520. IAEA.

Gauthier-Lafaye, F. (1986) Les gisements d'uranium du Gabon et les réacteurs d'Oklo. Modèle métallogénique de gites à fortes teneurs du Protérozoique inférieur. Mémoire Sciences Géologiques, 78–206.

Gauthier-Lafaye F. and Weber F. (1989) The Francevillian (lower Proterozoic) uranium ore deposits of Gabon. *J. Econ. Geol.* **84,** 2267–2285.

Gauthier-Lafaye F., Holliger P. and Blanc P.-L. (1996) Natural fission reactors in the Franceville basin, Gabon: A review of the conditions and results of a ''critical event'' in a geologic system. *Geochim. Cosmochim. Acta* **60**, 4831–4852.

Hidaka H., Shinotsuka K. and Holliger P. (1993) Geochemical behaviour of $^{99}$Tc in the Oklo natural fission reactors. *Radiochim. Acta* **63**, 19–22.

Hidaka H., Sugiyama T., Ebihara M. and Holliger P. (1994) Isotopic evidence for the retention of $^{90}$Sr inferred from excess $^{90}$Zr in the Oklo natural fission reactors: Implication for geochemical behaviour of fissiogenic Rb, Sr, Cs and Ba. *Earth Plan. Sci. Lett.* **122**, 173–182.

Hidaka H. and Holliger P. (1998) Geochemical and neutronic characteristics of the natural fossil fission reactors at Oklo and Bangombé Gabon. *Geochim. Cosmochim. Acta* **62**, 89–108.

Hidaka H., Holliger P. and Gauthier-Lafaye F. (1999) Tc/Ru fractionation in the Oklo and Bangombé natural fission reactors, Gabon. *Chem. Geol.* **155**, 323–333.

Holliger, P. (1988) Ages U–Pb définis in-situ sur oxides d'uranium à l'analyseur ionique: méthodologie et consé- quences géochimiques. *C.R. Acad. Sci. Paris* **307**, 367–373.

Holliger P. (1992) Les nouvelles zones de réaction d'Oklo: Datation U-Pb et caractérisation in-situ des produits de fission à l'analyseeur ionique. Programme "Oklo-Analogues Naturels," Note technique CEN Grenoble DEM n°01/92. Commissariat à l'Energie Atomique.

Holliger P. (1993) SIMS studies on the Oklo natural fission reactors. *Proc. SIMS IX Conference, Yokohama*, (Invited lecture) pp. 8–12.

Holliger P. (1994) Terme source: Caractérisation isotopique, paramètres nucléaires et modé1isation. Rapport CCE n°F112W-CT91-0071. Programme Oklo-Analogues

Naturels.

Holliger P. and Devillers C. (1981) Contribution a l'etude de la temperature dans les reacteurs fossils d'Oklo par la mesure du rapport isotopique du lutetium. *Earth. Planet. Sci. Lett.* **52**, 76–84.

Horie K., Hidaka H. and Gauthier-Lafaye F. (2004) Isotopic evidence for trapped fissiogenic REE and nucleogenic Pu in apatite and Pb evolution at the Oklo natural reactor. *Geochim. Cosmochim. Acta* **68**, 115–125.

Janeczek J. (1999) Mineralogy and geochemistry of natural fission reactors in Gabon. *Rev. Mineral.* **38,** 321–392.

Janeczek J. and Ewing R. (1996a) Florencite-(La) with fissiogenic REEs from a natural fission reactor at Bangombé, Gabon. *Am. Mineral.* **81,** 1263–1269.

Janeczek J. and Ewing R. (1996b) Phosphatian coffinite with rare earth elements and Ce-rich françoisite-(Nd) from sandstone beneath a natural fission reactor at Bangombé, Gabon. *Mineral. Mag.* **60,** 665–669.

Kleykamp K. (1985) The chemical state of fission products in oxide fuels. *J. Nucl. Mat.* **131**, 221–246.

Loss R. D., Rosman K. J. R., DeLaeter J. R., Curtis D. B., Benjamin T. M., Gancarz A. J., Maeck W. J. and Delmore J. E. (1989) Fission-product retentivity in peripheral rocks at the Oklo natural fission reactors. Gabon. *Chem. Geol.* **76**, 71–84.

Maravic H. Von and Smellie J. A. T. (1992) Alligator River Analogue Project Final Workshop, EUR proceedings of the 5th CEC Natural Analogue Working Group, Toledo, Spain. Oct. 5–8.

Mathieu R., Zetterström L., Cuney M., Gauthier-Lafaye F. and Hidaka H. (2001) Alteration of monazite and zircon and lead migration as geochemical tracers of fluid paleocirculations around the Oklo–Okléobondo and Bamgombé natural nuclear reaction zones (Franceville basin, Gabon). *Chem. Geol.* **171**, 147–171.

Minster J. F. and Ricard L. P. (1981) The isotopic composition of zirconium. *Int. J. Mass Spectrom. Ion Phys.* **37**, 259–272.

Nagy B., Gauthier-Lafaye F., Holliger P., Mossman D., Leventhal J. and Rigali M. (1993) Role of organic matter in the Proterozoic Oklo natural fission reactors, Gabon, Africa. *Geology* **21**, 655–658.

Naudet, R. (1991) Oklo: des réacteurs nucléaires fossiles. *Paris: Collection du Commissariat à l'Energie Atomique*. p. 695.

Naudet R. and Renson C. (1975) Résultats des analyses systématiques de teneurs isotopiques de l'uranium. Proc. *The Oklo Phenomenon,* pp. 265–288. IAEA.

Neuilly M., Bussac J., Fréjacques C., Nief G., Vendryes G. and Yvon J. (1972) Sur l'existence dans un passé reculé d'une réaction en chaine naturelle de fission, dans le gisement d'uranium d'Oklo (Gabon). *C. R. Acad. Sci. Paris* **275,** 1847–1849.

Nilsson S. and Jonsson M. (2008) On the catalytic effects of $UO_2$(s) and Pd(s) on the reaction between $H_2O_2$ and $H_2$ in aqueous solution. *J. Nucl. Mater.* **372**, 160–163.

Openshaw R., Pagel M. and Poty B. (1978) Phases fluids contemporaines de la diagenesé des grés, des mouvements tectoniques et du fonctionment des réacteurs nucléaires d'Oklo (Gabon). *The Natural Fission Reactors.* 267-296. IAEA.

Poths H., Schmitt-Strecker S. and Begemann F. (1987) On the isotopic composition of ruthenium in the Allende and Leoville carbonaceous chondrites. *Geochim. Cosmochim. Acta* **51**, 1143–1149.

Ruffenach, J. C. (1979) Les réacteurs nucléaires naturels d'Oklo. Paramètres neutroniques, date et durée de fonctionnement, migrations de l'uranium et des produits de fission. Ph.D. dissertation, Univ. Paris VII.

Ruffenach J. C., Hagemann R. and Roth E. (1980) Isotopic abundances measurements: A key to understanding the Oklo Phenomenon. *Zeit. Naturforsch* **35a**, 171–179.

Röllin S.**,** Spahiu K. and Eklund U. -B. (2001) Determination of dissolution rates of spent fuel in carbonate solutions under different redox conditions with a flow-through experiment. *J. Nucl. Mater.* **297**, 231–243.

Savary V. and Pagel M, (1997) The effects of water radiolysis on local redox conditions in the Oklo, Gabon, natural fission reactors 10 and 16. *Geochim. Cosmochim. Acta* **61,**

4479-4494.

Stille P., Gauthier-Lafaye F., Jensen K. A., Salah S., Bracke G., Ewing R. C., Louvat D., and Million D. (2003) REE mobility in groundwater proximate to the natural fission reactor at Bangombé (Gabon). *Chem. Geol*. **198,** 289–304.

Thomas L. E. and Guenther R. J. (1989) Characterization of low-gas-release LWR fuels by transmission electron microscopy. In *Scientific Basis for Nuclear Waste Management XII.* (eds. W. Lutze and R. C. Ewing). *Mater. Res. Soc. Symp. Proc.* **127,** 293.

Utsunomiya S. and Ewing R. C. (2006) The fate of the epsilon phase (Mo-Ru-Pd-Tc-Rh) in the $UO_2$ of the Oklo natural fission reactors. *Radiochim. Acta* **94**, 749-753.

Wieser M. E., De Laeter J. R. and Varner M. D. (2007) Isotope fractionation studies of molybdenum. *Int. J. Mass Spectrom.* **265**, 40–48.

Table 1
Chemical compositions (weight percentage) of metallic aggregates in SD37-S2/CD, RZ13.

| No. | Ru | Rh | Pd | Te | Pb | U | As | S | Bi | Sb | Ni | Cu | Total |
|---|---|---|---|---|---|---|---|---|---|---|---|---|---|
| 1 | 49.33 | 7.06 | 1.12 | 4.39 | 2.66 | 0.21 | 14.02 | 2.21 | 4.17 | 0.64 | 0.61 | 0.20 | 86.63 |
| 2 | 58.73 | 6.97 | 2.00 | 2.48 | 1.46 | 0.10 | 9.58 | 1.68 | 2.46 | 0.38 | 0.53 | 0.30 | 86.65 |
| 3 | 48.93 | 5.21 | 1.34 | 3.07 | 3.20 | 0.15 | 20.20 | 1.63 | 4.85 | 0.77 | 1.15 | 0.16 | 90.66 |
| 4 | 56.37 | 4.38 | 1.12 | 2.23 | 2.74 | 0.18 | 15.33 | 1.26 | 3.65 | 0.69 | 1.23 | 0.38 | 89.56 |
| 5 | 61.60 | 4.99 | 1.03 | 2.43 | 2.11 | 0.08 | 11.23 | 1.54 | 2.28 | 0.45 | 0.85 | 0.53 | 89.10 |
| 6 | 61.64 | 4.13 | 0.88 | 2.10 | 1.59 | 0.04 | 9.66 | 1.52 | 1.89 | 0.40 | 0.89 | 0.47 | 85.21 |
| 7 | 50.56 | 6.74 | 1.19 | 4.26 | 2.72 | 0.25 | 14.83 | 2.07 | 4.40 | 0.72 | 0.64 | 0.28 | 88.66 |
| 8 | 49.34 | 5.69 | 0.77 | 4.70 | 2.57 | 0.27 | 14.03 | 2.33 | 4.70 | 0.59 | 0.58 | 0.19 | 85.76 |
| 9 | 35.44 | 7.66 | 1.97 | 4.77 | 4.31 | 0.16 | 24.07 | 1.39 | 5.00 | 0.90 | 1.08 | < 0.01 | 86.74 |
| 10 | 38.55 | 7.11 | 2.02 | 3.74 | 4.11 | 0.25 | 28.54 | 1.41 | 4.04 | 0.61 | 1.19 | < 0.01 | 91.58 |
| 11 | 46.16 | 8.71 | 1.22 | 5.23 | 2.94 | 0.32 | 19.57 | 2.25 | 5.06 | 0.76 | 0.69 | 0.08 | 92.97 |
| 12 | 48.77 | 7.62 | 1.19 | 5.10 | 2.55 | 0.26 | 19.19 | 2.65 | 4.70 | 0.68 | 0.69 | 0.08 | 93.46 |
| 13 | 62.34 | 5.41 | 0.92 | 2.99 | 1.88 | 0.20 | 10.97 | 2.08 | 2.63 | 0.31 | 0.55 | 0.37 | 90.64 |
| 14 | 51.10 | 6.55 | 1.11 | 3.45 | 2.56 | 0.24 | 14.93 | 2.09 | 3.98 | 0.60 | 0.83 | 0.21 | 87.63 |
| 15 | 68.98 | 4.12 | 1.42 | 1.62 | 1.24 | 0.07 | 6.36 | 1.33 | 1.32 | 0.25 | 0.46 | 0.47 | 87.65 |
| 16 | 54.26 | 6.08 | 1.14 | 4.26 | 2.20 | 0.16 | 12.09 | 2.24 | 4.08 | 0.49 | 0.52 | 0.26 | 87.78 |
| 17 | 43.81 | 7.78 | 1.24 | 5.93 | 3.00 | 0.25 | 18.85 | 2.41 | 5.33 | 0.75 | 0.71 | 0.10 | 90.14 |
| 18 | 43.85 | 5.90 | 1.54 | 4.21 | 4.29 | 0.36 | 23.36 | 1.85 | 5.66 | 0.69 | 1.11 | 0.11 | 92.93 |
| 19 | 45.03 | 5.19 | 1.41 | 4.14 | 4.07 | 0.21 | 23.46 | 2.06 | 5.70 | 0.71 | 1.13 | 0.10 | 93.18 |
| 20 | 50.79 | 4.83 | 1.26 | 3.54 | 3.75 | 0.24 | 21.23 | 2.02 | 3.94 | 0.68 | 1.12 | 0.24 | 93.63 |
| 21 | 41.84 | 8.30 | 1.29 | 5.23 | 4.49 | 0.39 | 19.89 | 2.26 | 7.97 | 0.70 | 0.69 | 0.04 | 93.08 |
| 22 | 51.87 | 6.73 | 1.10 | 3.61 | 3.03 | 0.15 | 16.74 | 2.15 | 5.35 | 0.66 | 0.91 | 0.20 | 92.51 |
| SD37-S2/CD[a] | 33.51 | 4.64 | n.r. | 2.71 | 38.89 | 0.39 | 7.99 | 7.43 | n.r. | n.r. | n.r. | n.r. | 95.55 |
| SF29[b] | 25.06 | 4.63 | n.r. | 0.70 | 20.51 | 1.42 | 31.29 | 11.62 | n.r. | n.r. | n.r. | n.r. | 95.32 |

[a]Average chemical composition of metallic aggregates in SD37-S2/CD in previous work. Data are from Hidaka et al. (1999).

[b]Average chemical composition of metallic aggregates in SF29 (RZ10). Data are from Gauthier-Lafaye et al. (1996).

n.r. = no reported.

Table 2
Pb and U isotopic ratios of the metallic aggregates in SD37-S2/CD.

| | $^{204}Pb/^{206}Pb$ | $^{207}Pb/^{206}Pb$ | $^{208}Pb/^{206}Pb$ | $^{235}U/^{238}U$ | $^{207}Pb/^{206}Pb$[a] | $^{207}Pb/^{206}Pb$[b] | Age (Ma)[b] |
|---|---|---|---|---|---|---|---|
| SD37-S2/CD | | | | | | | |
| Metallic aggregate | | | | | | | |
| 1-1 | 0.000149 ± 0.000012 | 0.103 ± 0.006 | 0.00824 ± 0.00050 | 0.00500 ± 0.00016 | 0.101 ± 0.010 | 0.146 ± 0.015 | 2304 ± 179 |
| 1-2 | 0.000131 ± 0.000015 | 0.091 ± 0.009 | 0.00715 ± 0.00072 | 0.00478 ± 0.00015 | 0.089 ± 0.013 | 0.135 ± 0.021 | 2167 ± 269 |
| 2-1 | N.A. | N.A. | N.A. | 0.00555 ± 0.00017 | | | |
| 3-1 | N.A. | N.A. | N.A. | 0.00549 ± 0.00016 | | | |
| 3-2 | N.A. | N.A. | N.A. | 0.00523 ± 0.00015 | | | |
| 4-1 | 0.000171 ± 0.000005 | 0.104 ± 0.001 | 0.00847 ± 0.00009 | 0.00720 ± 0.00023 | 0.102 ± 0.003 | 0.102 ± 0.005 | 1667 ± 82 |
| 5-1 | 0.000178 ± 0.000006 | 0.109 ± 0.001 | 0.00875 ± 0.00007 | 0.00497 ± 0.00015 | 0.107 ± 0.004 | 0.155 ± 0.007 | 2407 ± 78 |
| 5-2 | 0.000217 ± 0.000014 | 0.110 ± 0.003 | 0.00892 ± 0.00023 | 0.00930 ± 0.00030 | 0.107 ± 0.007 | 0.083 ± 0.006 | 1279 ± 150 |
| 5-3 | 0.000139 ± 0.000011 | 0.103 ± 0.009 | 0.00673 ± 0.00059 | N.A. | 0.101 ± 0.012 | | |
| 6-1 | 0.000176 ± 0.000013 | 0.106 ± 0.006 | 0.00803 ± 0.00046 | 0.01252 ± 0.00040 | 0.104 ± 0.010 | 0.060 ± 0.006 | 603 ± 213 |
| 6-2 | N.A. | N.A. | N.A. | 0.00978 ± 0.00031 | | | |
| 6-3 | N.A. | N.A. | N.A. | 0.00622 ± 0.00020 | | | |
| 8-1 | 0.000175 ± 0.000004 | 0.114 ± 0.002 | 0.00802 ± 0.00014 | 0.00968 ± 0.00031 | 0.112 ± 0.003 | 0.084 ± 0.004 | 1283 ± 84 |
| 8-2 | 0.000164 ± 0.000007 | 0.114 ± 0.005 | 0.00793 ± 0.00030 | N.A. | 0.112 ± 0.007 | | |
| 9-1 | 0.000184 ± 0.000020 | 0.109 ± 0.004 | 0.00792 ± 0.00066 | 0.00771 ± 0.00025 | 0.106 ± 0.012 | 0.100 ± 0.012 | 1626 ± 222 |
| 10-1 | 0.000142 ± 0.000013 | 0.099 ± 0.009 | 0.00732 ± 0.00070 | 0.00568 ± 0.00018 | 0.097 ± 0.013 | 0.124 ± 0.016 | 2012 ± 236 |
| 10-2 | 0.000158 ± 0.000005 | 0.105 ± 0.003 | 0.00755 ± 0.00025 | N.A. | 0.103 ± 0.004 | | |
| 11-1 | 0.000185 ± 0.000008 | 0.114 ± 0.005 | 0.00856 ± 0.00035 | 0.00870 ± 0.00028 | 0.111 ± 0.007 | 0.093 ± 0.006 | 1486 ± 132 |
| 11-2 | 0.000164 ± 0.000009 | 0.104 ± 0.007 | 0.00791 ± 0.00050 | N.A. | 0.102 ± 0.009 | | |
| 12-1 | 0.000155 ± 0.000008 | 0.110 ± 0.006 | 0.00758 ± 0.00040 | 0.00711 ± 0.00021 | 0.108 ± 0.008 | 0.110 ± 0.009 | 1799 ± 147 |
| 12-2 | 0.000162 ± 0.000003 | 0.109 ± 0.001 | 0.00754 ± 0.00008 | 0.00885 ± 0.00026 | 0.107 ± 0.002 | 0.087 ± 0.003 | 1371 ± 69 |
| 12-3 | 0.000153 ± 0.000004 | 0.109 ± 0.003 | 0.00738 ± 0.00021 | 0.00724 ± 0.00023 | 0.107 ± 0.004 | 0.107 ± 0.005 | 1750 ± 91 |
| 12-4 | N.A. | N.A. | N.A. | 0.00663 ± 0.00021 | | | |
| 13-1 | 0.000135 ± 0.000008 | 0.098 ± 0.004 | 0.00726 ± 0.00033 | 0.00503 ± 0.00016 | 0.096 ± 0.007 | 0.139 ± 0.011 | 2209 ± 137 |
| 13-2 | 0.000140 ± 0.000011 | 0.098 ± 0.008 | 0.00722 ± 0.00065 | 0.00514 ± 0.00016 | 0.096 ± 0.011 | 0.135 ± 0.016 | 2170 ± 205 |
| 14-1 | 0.000208 ± 0.000011 | 0.121 ± 0.001 | 0.00894 ± 0.00009 | 0.01466 ± 0.00046 | 0.118 ± 0.006 | 0.058 ± 0.004 | 547 ± 136 |
| 14-2 | 0.000180 ± 0.000006 | 0.111 ± 0.003 | 0.00827 ± 0.00023 | N.A. | 0.109 ± 0.011 | | |
| SD37-S2/CD2[c] | <0.0005 | 0.12660 | 0.01413 | | | | |
| SD37-S2/CD5[c] | <0.0005 | 0.12590 | 0.01376 | | | | |

Analytical errors are 1σ of the mean. N.A. = not analyzed in this study.

[a]Isotopic composition of radiogenic lead. Correction for common lead: $^{206}Pb/^{204}Pb$ = 18.61. $^{207}Pb/^{204}Pb$ = 15.75. (Mathieu et al., 2001).

[b]Isotopic composition of radiogenic lead and apparent age after correction for $^{235}U$ depletion and enrichment.

[c]The two data of the metallic aggregates in SD37-S2/CD are from Gauthier-Lafaye et al. (1996).

Table 3
Zr, Mo and Ru isotopic ratios of the metallic aggregates in SD37-S2/CD.

| | $^{90}Zr/^{91}Zr$ | $^{97}Mo/^{95}Mo$ | $^{99}Ru/^{101}Ru$ |
|---|---|---|---|
| SD37-S2/CD | | | |
| Metallic aggregate | | | |
| 1-1 | 1.731 ± 0.005 | 0.921 ± 0.007 | 0.838 ± 0.008 |
| 1-2 | 1.743 ± 0.011 | 0.919 ± 0.006 | 0.912 ± 0.009 |
| 1-3 | 1.744 ± 0.008 | 0.918 ± 0.004 | 0.780 ± 0.008 |
| 1-4 | 1.721 ± 0.006 | 0.931 ± 0.007 | 0.620 ± 0.007 |
| 2-1 | 2.113 ± 0.035 | 0.902 ± 0.004 | 0.636 ± 0.003 |
| 2-2 | 2.651 ± 0.028 | 0.891 ± 0.010 | 0.563 ± 0.006 |
| 3-1 | 1.788 ± 0.010 | 0.932 ± 0.005 | 0.614 ± 0.007 |
| 3-2 | 2.093 ± 0.040 | 0.929 ± 0.011 | 0.807 ± 0.010 |
| 4-1 | 1.737 ± 0.011 | 0.912 ± 0.004 | 0.577 ± 0.006 |
| 4-2 | 1.843 ± 0.051 | 0.911 ± 0.006 | 0.582 ± 0.002 |
| 5-1 | 1.887 ± 0.020 | 0.922 ± 0.004 | 1.657 ± 0.012 |
| 5-2 | 1.858 ± 0.024 | 0.910 ± 0.003 | 1.725 ± 0.029 |
| 6-1 | 1.790 ± 0.010 | 0.900 ± 0.010 | 0.689 ± 0.009 |
| 6-2 | 1.801 ± 0.017 | 0.913 ± 0.007 | 0.746 ± 0.012 |
| 7-1 | 1.765 ± 0.009 | 0.898 ± 0.003 | 0.324 ± 0.001 |
| 7-2 | 1.774 ± 0.007 | 0.899 ± 0.007 | 0.331 ± 0.001 |
| 8-1 | 1.708 ± 0.009 | 0.910 ± 0.005 | 1.216 ± 0.014 |
| 8-2 | 1.741 ± 0.011 | 0.903 ± 0.004 | 1.216 ± 0.004 |
| 9-1 | 1.707 ± 0.005 | 0.897 ± 0.003 | 1.256 ± 0.010 |
| 9-2 | 1.698 ± 0.006 | 0.898 ± 0.003 | 1.207 ± 0.003 |
| 10-1 | 1.811 ± 0.010 | 0.912 ± 0.004 | 0.653 ± 0.003 |
| 10-2 | 1.814 ± 0.002 | 0.909 ± 0.005 | 0.677 ± 0.001 |
| 11-1 | 1.769 ± 0.004 | 0.817 ± 0.005 | 1.020 ± 0.016 |
| 11-2 | 1.754 ± 0.006 | 0.892 ± 0.004 | 0.963 ± 0.003 |
| 12-1 | 1.702 ± 0.046 | 0.882 ± 0.004 | 1.034 ± 0.004 |
| 12-2 | 1.661 ± 0.009 | 0.883 ± 0.005 | 1.080 ± 0.005 |
| 13-1 | 1.692 ± 0.004 | 0.917 ± 0.002 | 1.214 ± 0.017 |
| 13-2 | 1.708 ± 0.005 | 0.915 ± 0.004 | 1.372 ± 0.004 |
| 14-1 | 1.648 ± 0.008 | 0.906 ± 0.006 | 1.056 ± 0.008 |
| 14-2 | 1.725 ± 0.010 | 0.882 ± 0.001 | 1.080 ± 0.002 |
| SD37-S2/CD.2[a] | N.A. | N.A. | 1.9342 |
| SD37-S2/CD.3[a] | N.A. | N.A. | 1.5611 |
| SD37-S2/CD.5[a] | N.A. | N.A. | 2.2842 |
| STD | 4.659 ± 0.004 | 0.5986 ± 0.0002 | 0.7550 ± 0.0005 |
| Fissiogenic[b] | 0.9456 | 0.9768 | 1.136 |

N.A. = not analyzed.
Analytical uncertainties are 1σ of the mean.
[a]The data of the metallic aggregates in SD37-S2/CD are from Hidaka et al. (1999).
[b]Fissiogenic values are obtained after consideration of the fission yields of nuclides of Zr, Mo and Ru (England and Rider, 1988) and fission contributions of $^{235}U$, $^{238}U$ and $^{239}Pu$ in SD37-S2/CD (Hidaka et al., 1999).

Figure captions

Figure 1. (a) The location of Oklo reactor zones. (b) Cross section of the deposit with the depth location of the reactor zone. (c) Cross section of gallery SD37 at reactor zone 13.

Figure 2. Backscattered electron (BSE) image of typical metallic aggregates having micro-inclusions (a) and relatively homogeneous distribution (b) in this study. The scale bar is 10 μm.

Figure 3. Plots of As content vs. Ru content (a), As content vs. Pd content (b), and Cu content vs. Ru content (c) of the metallic aggregates investigated in this study.

Figure 4. Isotopic ratios of $^{235}U/^{238}U$ for the metallic aggregates investigated in this study. The isotopic data are lined up in chronological order. The dotted line shows the terrestrial $^{235}U/^{238}U$ ratio obtained from standard zircon AS3 (0.00725±0.00004).

Figure 5. $^{204}Pb/^{206}Pb$ vs. $^{207}Pb/^{206}Pb$ diagram of the metallic aggregates investigated in this study (●). For purposes of comparison, the data of uraninite (□) and galena (△) in RZ 13 and metal Pb (○) in RZ10 (Gauthier-Lafaye et al., 1996) are also shown.

Figure 6. $^{235}U/^{238}U$ vs. $^{207}Pb/^{206}Pb$ diagram of the metallic aggregates investigated in this study. “f” values in the figure show proportion of the non-fractionated U and Pb component relative to the total fraction. The definition is provided in the text.

Figure 7. Isotopic ratios of $^{90}Zr/^{91}Zr$ (a), $^{95}Mo/^{97}Mo$ (b) and $^{99}Ru/^{101}Ru$ (c) for the metallic aggregates investigated in this study. The isotopic data in each figure are lined up in chronological order and the corresponding analytical numbers in (a), (b) and (c) mean the same analytical spots in SHRIMP analyses. The dotted lines in each of the figures show the isotopic ratios of fissiogenic Zr, Mo, Ru (0.9456, 0.9768 and 1.136). On the other hand, the solid lines show the isotopic ratios of non-fissiogenic Zr, Mo and Ru determined from the standard material (4.659±0.004, 0.5986±0.0002 and 0.7550±0.0005). The shaded area indicates the expected isotopic ratios that could result from a mixing between fissiogenic and non-fissiogenic Zr, Mo and Ru.

Figure 8. The formation processes of the metallic aggregates in SD37-S2/CD at RZ 13.

Fig. 1. Kikuchi et al.

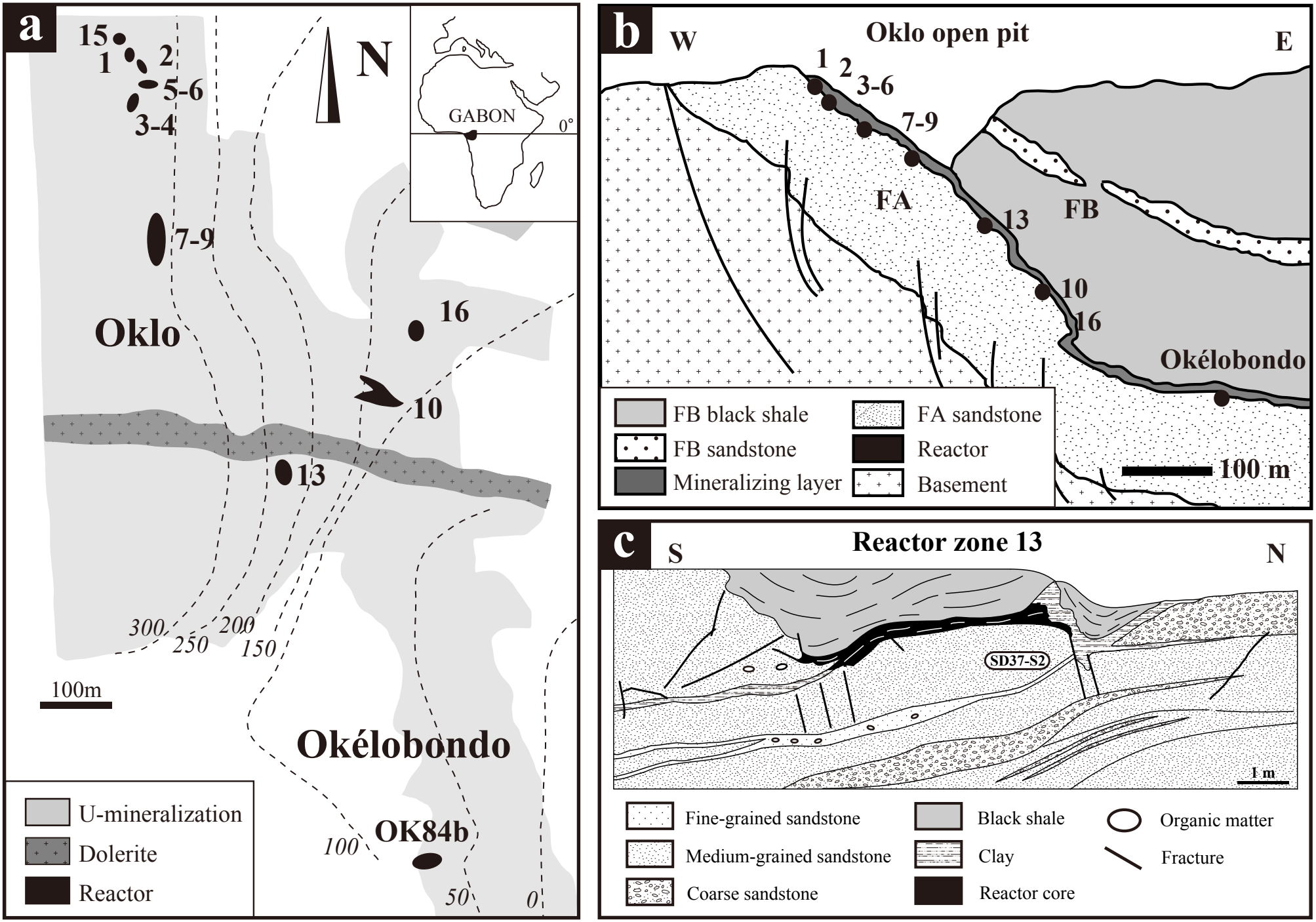

Fig. 2. Kikuchi et al.

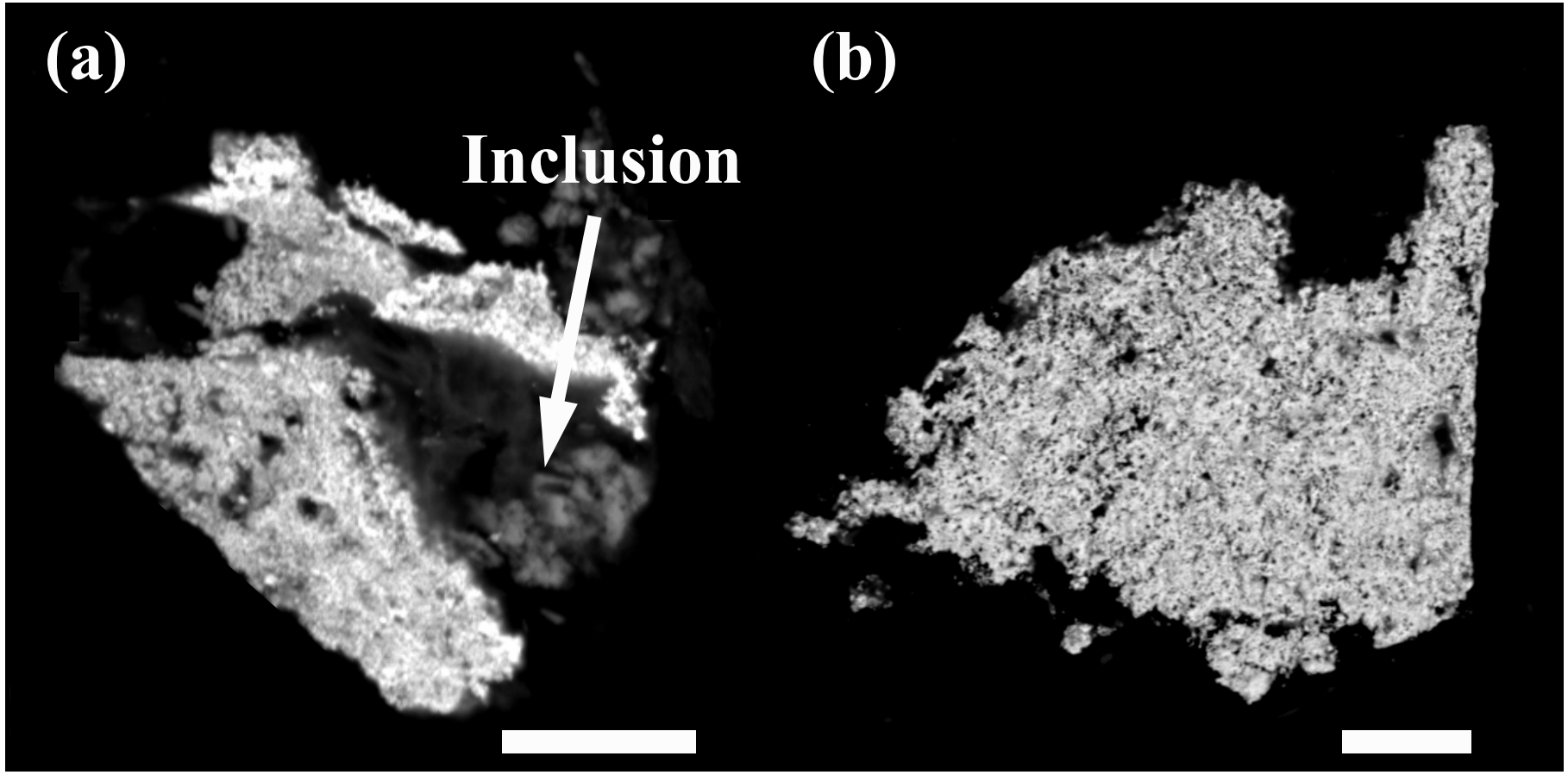

Fig. 3 Kikuchi et al.

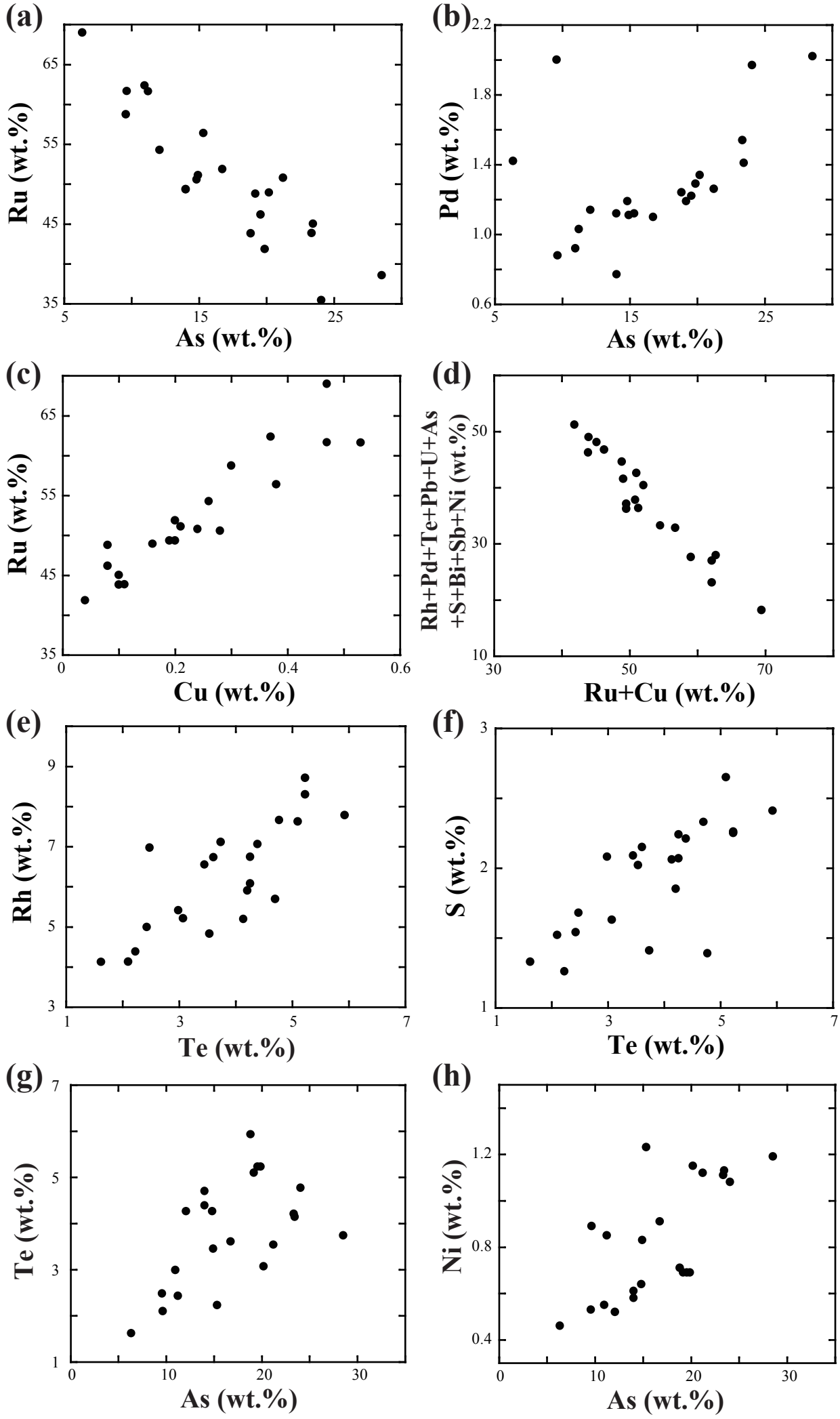

Fig. 4. Kikuchi et al.

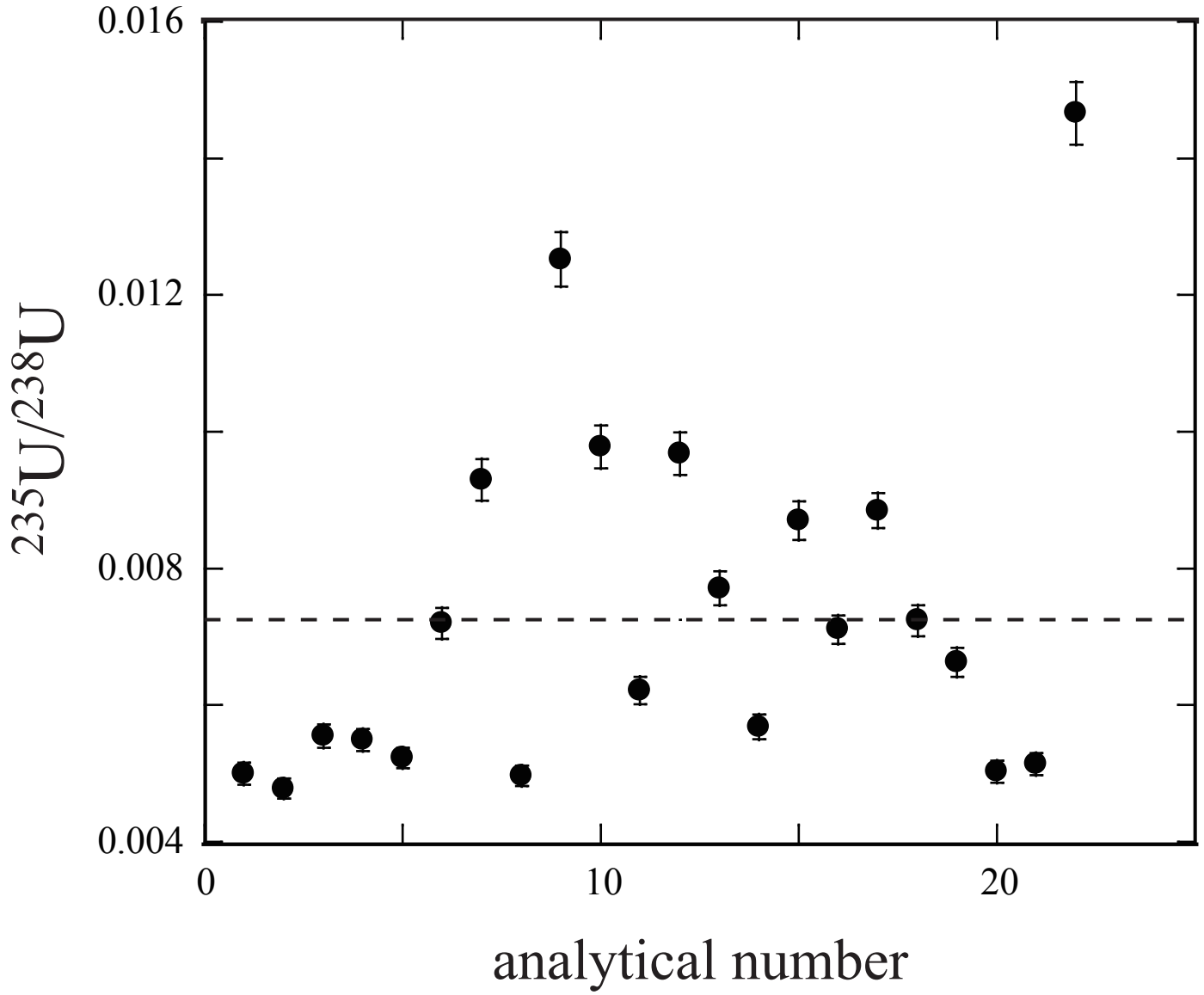

Fig. 5. Kikuchi et al.

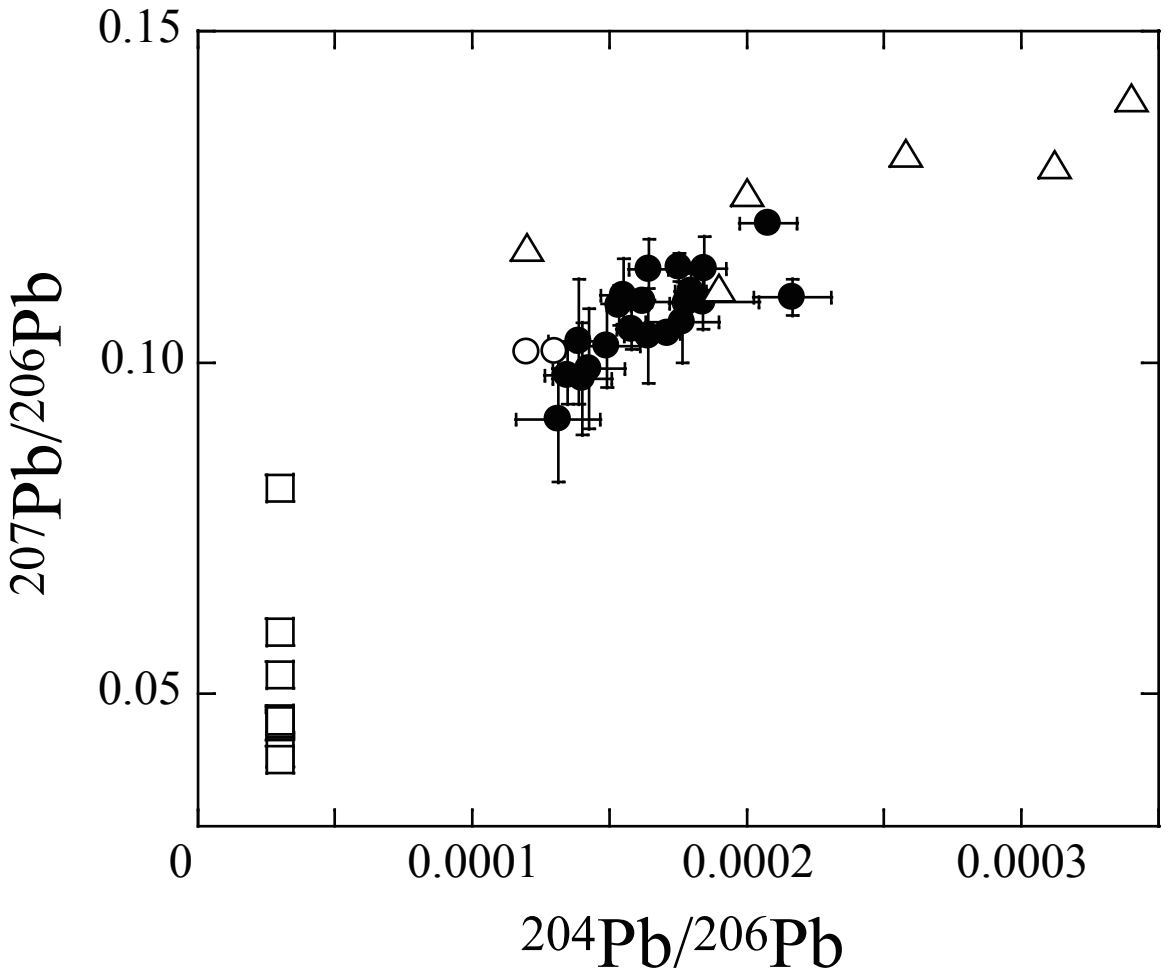

Fig. 6. Kikuchi et al.

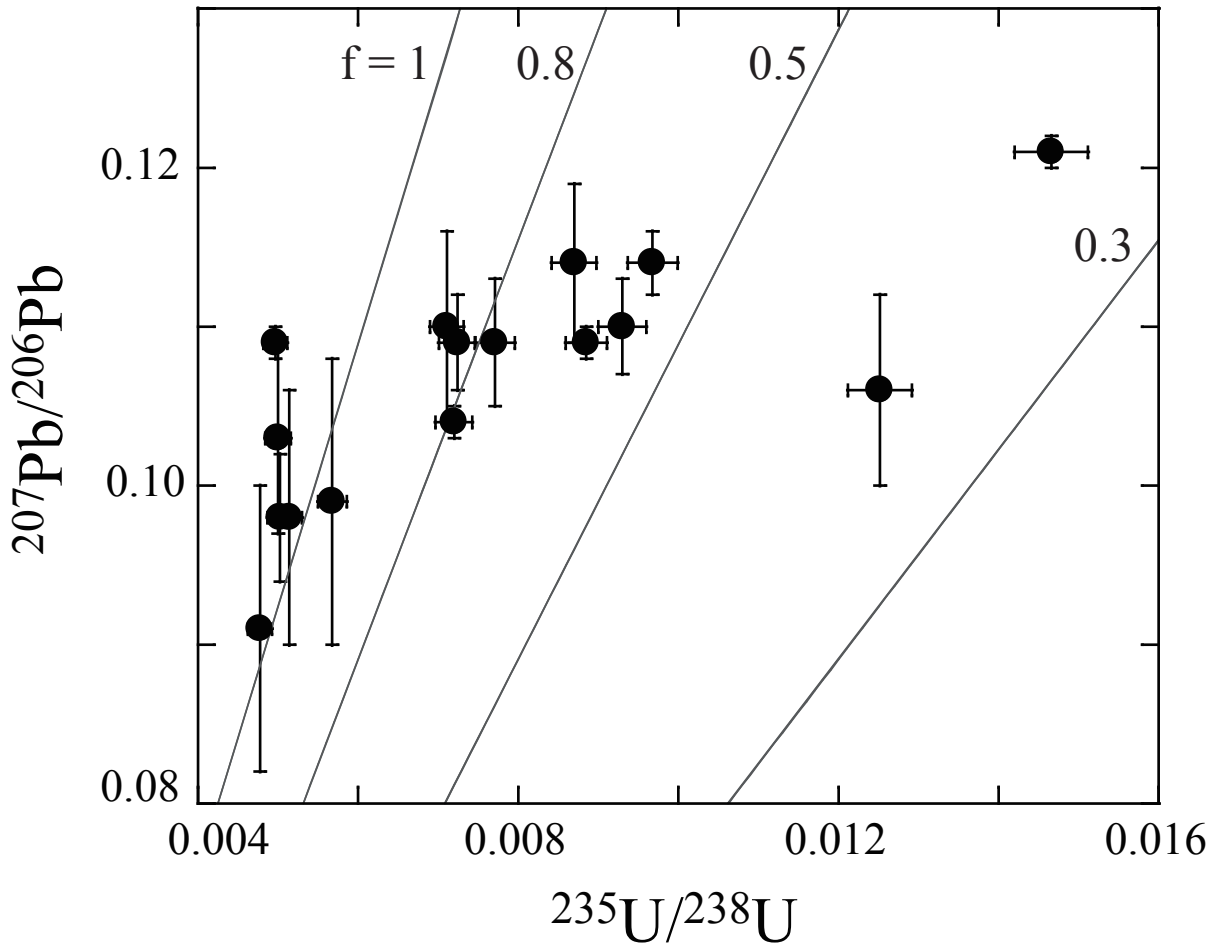

Fig. 7. Kikuchi et al.

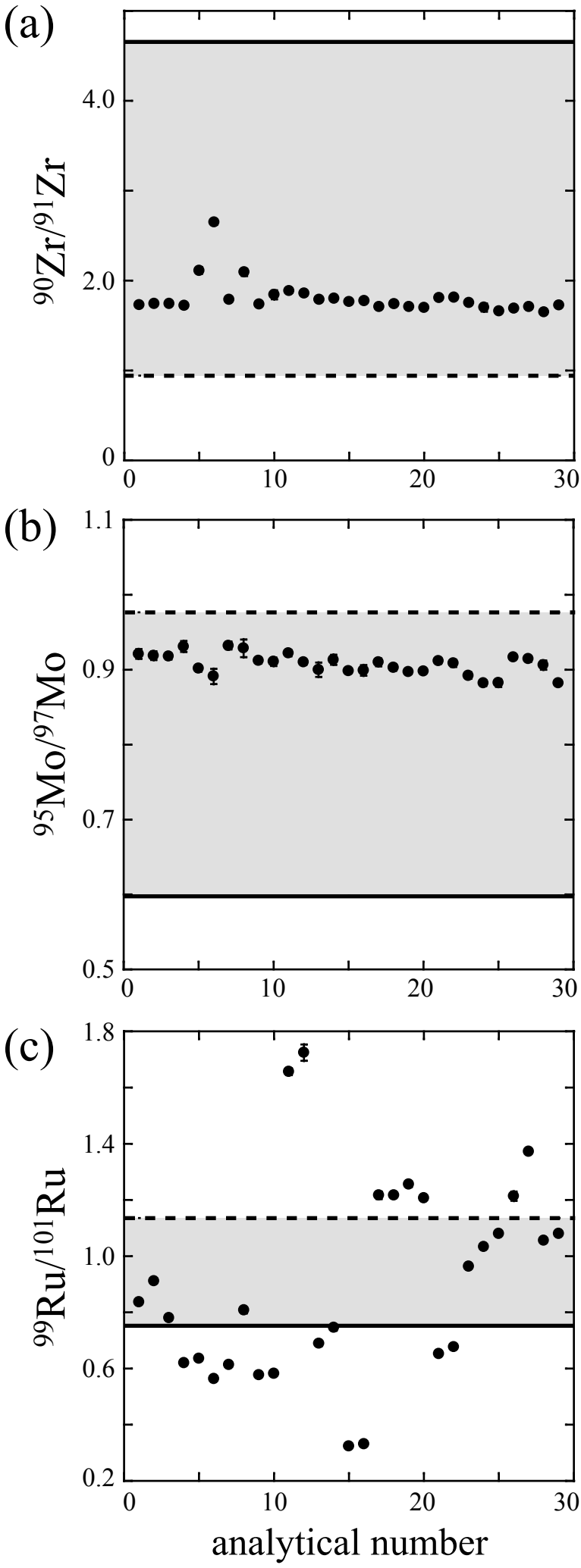

Fig. 8. Kikuchi et al.